Effects of magnetic dopants in (Li_{0.8}M_{0.2}OH)FeSe (M=Fe, Mn, Co): Density functional theory study using a band unfolding technique

M. X. Chen, Wei Chen, Zhenyu Zhang, and M. Weinert

Effects of magnetic dopants in $(\mathrm{Li}_{0.8}\mathrm{M}_{0.2}\mathrm{OH})\mathrm{FeSe}$ (M = Fe, Mn, Co): a density-functional theory study using band unfolding technique

M. X. Chen,[1, 2] Wei Chen,[3, 4] Zhenyu Zhang,[4] and M. Weinert[2]

[1] *College of Physics and Information Science, Hunan Normal University, Changsha, Hunan 410018, China*
[2] *Department of Physics, University of Wisconsin, Milwaukee, Wisconsin 53211, USA*
[3] *Department of Physics and School of Engineering and Applied Sciences,*
Harvard University, Cambridge, Massachusetts 02138, USA
[4] *International Center for Quantum Design of Functional Materials (ICQD),*
Hefei National Laboratory for Physical Sciences at Microscale,
and Synergetic Innovation Center of Quantum Information and Quantum Physics,
University of Science and Technology of China, Hefei, Anhui 230026, China
(Dated: November 2, 2017)

The effects of Fe dopants on the electronic bands structure of $(\mathrm{Li}_{0.8}\mathrm{Fe}_{0.2}\mathrm{OH})\mathrm{FeSe}$ are investigated by a band unfolding (k-projection) technique and first-principles supercell calculations. Doping 20% Fe into the LiOH layers causes electron donation to the FeSe layers, significantly changing the profile of bands around the Fermi level. Because of the weak bonding between the LiOH and FeSe layers the magnetic configuration of the dopants has only minor effects on the band structure. The electronic bands for the surface FeSe layer of $(\mathrm{Li}_{0.8}\mathrm{Fe}_{0.2}\mathrm{OH})\mathrm{FeSe}$ show noticeable differences compared to those of the inner layers, both in the location of the Fermi level and in details of the bands near the high symmetry points, resulting from different effective doping levels and the broken symmetry at the surface. The band structure for the surface FeSe layer with checkerboard antiferromagnetic order is reasonably consistent with angle-resolved photoemission results. The $3d$ transition-metals Mn and Co have similar doping effects on the band structure of (LiOH)FeSe.

PACS numbers: 71.20.-b,73.20.-r,73.22.Pr

I. INTRODUCTION

The discovery of superconductivity in REFeAsO (RE = rare earth) compounds with T_c as high as 55 K has engendered significant interest in searching for new Fe-based superconductors. One surprise from these recent explorations is that an FeSe monolayer epitaxially grown on $\mathrm{SrTiO_3}$ shows superconducting T_c as high as 77 K,[1] much higher than its bulk phase. One unusual and puzzling feature of this system is that its Fermi surface is characterized by an electron-like pocket centered around the M points, while no pocket appears near the Γ point.[2–5] This observation challenges the Fermi surface nesting scenario that relies on nesting between M and Γ-point electronic states.[6,7] More recently, a superconducting T_c over 40 K was observed in an FeSe-based bulk phase, $(\mathrm{Li}_{1-x}\mathrm{Fe}_x\mathrm{OH})\mathrm{FeSe}$.[8–11] Unlike the binary FeSe compound, $(\mathrm{Li}_{1-x}\mathrm{Fe}_x)\mathrm{OH}$ layers are intercalated between the FeSe layers. This new type of FeSe-based superconductor is also distinct from the alkali-metal intercalated counterpart: it is stable at ambient condition, whereas the later is extremely sensitive to air. Moreover, magnetism was found to coexist with superconductivity in $\mathrm{Li}_{1-x}\mathrm{Fe}_x\mathrm{OH}$.[8,9] The angle-resolved photoemission spectroscopy (ARPES) experiments of Ref. [12] find that $(\mathrm{Li}_{0.8}\mathrm{Fe}_{0.2}\mathrm{OH})\mathrm{FeSe}$ has an electronic structure akin to that of $\mathrm{Rb}_{0.76}\mathrm{Fe}_{1.87}\mathrm{Se}_2$, with similar band dispersions and gap symmetry. In addition, ARPES experiments find that the band structure for $(\mathrm{Li}_{0.8}\mathrm{Fe}_{0.2}\mathrm{OH})\mathrm{FeSe}$ shares great similarities to that of $\mathrm{FeSe/SrTiO_3}$, suggesting that the superconductivity in this system and in $\mathrm{FeSe/SrTiO_3}$

may have a common electronic origin.[13]

Several density functional theory (DFT) calculations have been performed for $(\mathrm{Li}_{1-x}\mathrm{Fe}_x\mathrm{OH})\mathrm{FeSe}$.[13–15] However, the reported DFT-derived band structures are for nonmagnetic (LiOH)FeSe without the Fe dopants, and are found to be largely inconsistent with the ARPES measurements.[13,14] In particular, hole pockets near the Γ point seen in the DFT calculations, are actually absent in the ARPES measurements.[13,14] DFT supercell calculations carried out by some of us[15] find that the Fe dopants play an important role in the structural stability of $(\mathrm{Li}_{0.8}\mathrm{Fe}_{0.2}\mathrm{OH})\mathrm{FeSe}$, and the charge transfer between the LiOH and FeSe layers. Although both Refs. [8] and [9] find that the magnetism coexisting with the superconductivity originates from the Fe dopants, they report different kinds of magnetism, i.e., ferromagnetism vs antiferromagnetism. This discrepancy was also seen in the DFT calculations. The local-density approximation (LDA) calculations of Ref. [14] give ferromagnetically aligned Fe moments in the LiOH layers, while our calculations[15] using the Perdew-Burke-Ernzerhof GGA find that they are antiferromagnetically aligned. The different magnetic orderings found may originate from different configurations/distributions of Fe dopants since the energy difference between the AFM and FM coupling of the Fe dopants is small.[15] Moreover, our study[15] predicted that $(\mathrm{Li}_{0.8}\mathrm{Co}_{0.2}\mathrm{OH})\mathrm{FeSe}$ is structurally stable with even larger electron injection, possibly leading to a higher T_c. Intrinsically, spin-orbit coupling (SOC) also plays an important in the electronic properties of Fe-based superconductors,[16–18] including driving the FeSe
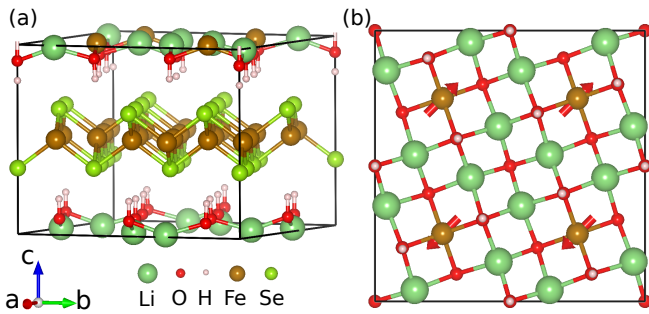
FIG. 1. Structural model of $(Li_{0.8}Fe_{0.2}OH)FeSe$. (a) Perspective view of $(Li_{0.8}Fe_{0.2}OH)FeSe$. (b) Top view of $Li_{0.8}Fe_{0.2}OH$ layer. The red arrows represent the relative magnetization of the Fe dopants in the collinear antiferromagnetic configuration. In addition to the collinear AFM configuration, checkerboard antiferromagnetic and ferromagnetic between the Fe dopants (not shown) are also investigated in the present study.

monolayers into nontrivial topological phases.[16] Dopants such as oxygen vacancies in the $SrTiO_3$ substrate also can affect the SOC spin splitting at the M point for the checkerboard antiferromagnetic state.[19] As a step to gaining a better understanding of the physics underlying the superconductivity of these systems, it is worthwhile investigating the effects of the dopants, magnetic ordering, SOC, and the interplay among them on the normal state band structure of $(Li_{0.8}Fe_{0.2}OH)FeSe$.

In this paper, we investigate the band structure of $(Li_{0.8}Fe_{0.2}OH)FeSe$ by carrying out DFT supercell calculations. The effects of the Fe dopants on the electronic bands are studied by means of a band unfolding technique that projects the supercell wave functions onto the k-points in the Brillouin zone of the 1×1 chemical unit cell of $(LiOH)FeSe$. We find that doping Fe into the LiOH layers not only shifts the Fermi level, but also induces significant changes in the profile of bands around the Fermi level. The magnetic ordering of the dopants in the LiOH layers, however, has only minor effects on the band structure. The band structure for the surface FeSe layer shows significant differences from those for inner layers in both the location of the Fermi level and band details near high symmetry points. We further investigate the band structures for Mn- and Co-doped $(Li_{0.8}M_{0.2}OH)FeSe$ (M = Mn and Co), and show that Fe, Mn, or Co doping has similar effects on the band structure of $(LiOH)FeSe$.

II. COMPUTATIONAL DETAILS

Our calculations were performed using the Vienna Ab Initio Simulation Package.[20,21] Our previous study examined the effects of different exchange-correlation functionals on the lattice parameter and found that the Perdew-Burke-Ernzerhof (PBE) functional without including the popular vdW corrections yields a reasonable description of the structural properties.[15] Therefore, in the present study the exchange-correlation functional

is approximated by the generalized gradient approximation as parametrized by PBE,[22] and the pseudopotentials were constructed by the projector augmented wave method.[23,24] A $3\times3\times1$ Monkhorst-Pack k-mesh was used to sample the BZ and a plane-wave energy cutoff of 400 eV was used for electronic structure calculations. For calculations of $(Li_{0.8}Fe_{0.2}OH)FeSe(001)$ a slab consisting of three FeSe layers and two $Li_{0.8}Fe_{0.2}OH$ layers was used, with the surface terminated by FeSe layers. The slab is separated from its periodic images by 10 Å vacuum regions and was fully relaxed with a threshold of 0.001 eV/Å for the residual force on each atom.

We adapt the structural models reported in Ref. [15] for $(Li_{0.8}Fe_{0.2}OH)FeSe$ (Fig. 1), a $\sqrt{10} \times \sqrt{10}$ supercell of $(LiOH)FeSe$ with four Li atoms replaced by Fe atoms. To eliminate the band foldings caused by the use of supercells, we project the supercell wave functions onto the corresponding momentum vector k of the primitive (chemical) unit cell[25,26] of $(LiOH)FeSe$ (two Fe atoms in the FeSe layer). In this way, the Fe dopants serve as a perturbation on the bands of $(LiOH)FeSe$, whose effect can be seen in k-projected weights given by $|\psi_{\mathbf{k}}(\mathbf{r})|^2$, where the wave function $\psi_{\mathbf{k}}$ is k-projected. In essence, the procedure is to find which $\mathbf{k}_p$ of the primitive cell each plane wave $e^{i(\mathbf{k}_s+\mathbf{G})\cdot\mathbf{r}}$ belongs to, i.e., for integers M_i and m_j, determining the fractional part κ_j that defines $\mathbf{k}_p$ of the primitive cell relative to $\mathbf{k}_s$ of the supercell:

$$\mathbf{G} = \sum_i M_i \mathbf{B}_i = \sum_j (m_j + \kappa_j)\mathbf{b}_j$$

$$= \sum_j \left(\sum_i M_i (\mathbf{B}_i \cdot \mathbf{a}_j) \right) \mathbf{b}_j,$$

with $\mathbf{a}_i \cdot \mathbf{b}_j = \delta_{ij}$, where $\mathbf{B}$ and $\mathbf{b}$ are the reciprocal lattice vectors of the supercell and the primitive cell, respectively.

III. RESULTS AND DISCUSSIONS

A. Unfolded bands of $(Li_{0.8}Fe_{0.2}OH)FeSe$

We considered three magnetic configurations for the FeSe layers: non-magnetic (NM), checkerboard antiferromagnetic (CB-AFM), and collinear antiferromagnetic (CL-AFM). For the Fe dopants in $Li_{0.8}Fe_{0.2}OH$, we considered the CB-AFM, CL-AFM, and ferromagnetic (FM) orderings. The magnetic ground state is found to have CL-AFM ordering of the Fe atoms in both the FeSe and $Li_{0.8}Fe_{0.2}OH$ layers, with the interlayer spins aligned parallel to each other.[15]

Figure 2 shows the k-projected bands for $(LiOH)FeSe$ with and without the Fe dopants, for CL-AFM ordered Fe dopants. The effects of the magnetic configuration of the Fe dopants on the band structure of $(Li_{0.8}Fe_{0.2}OH)FeSe$ will be discussed later. One prominent feature is that the Fermi level experiences an upward shift upon Fe doping.
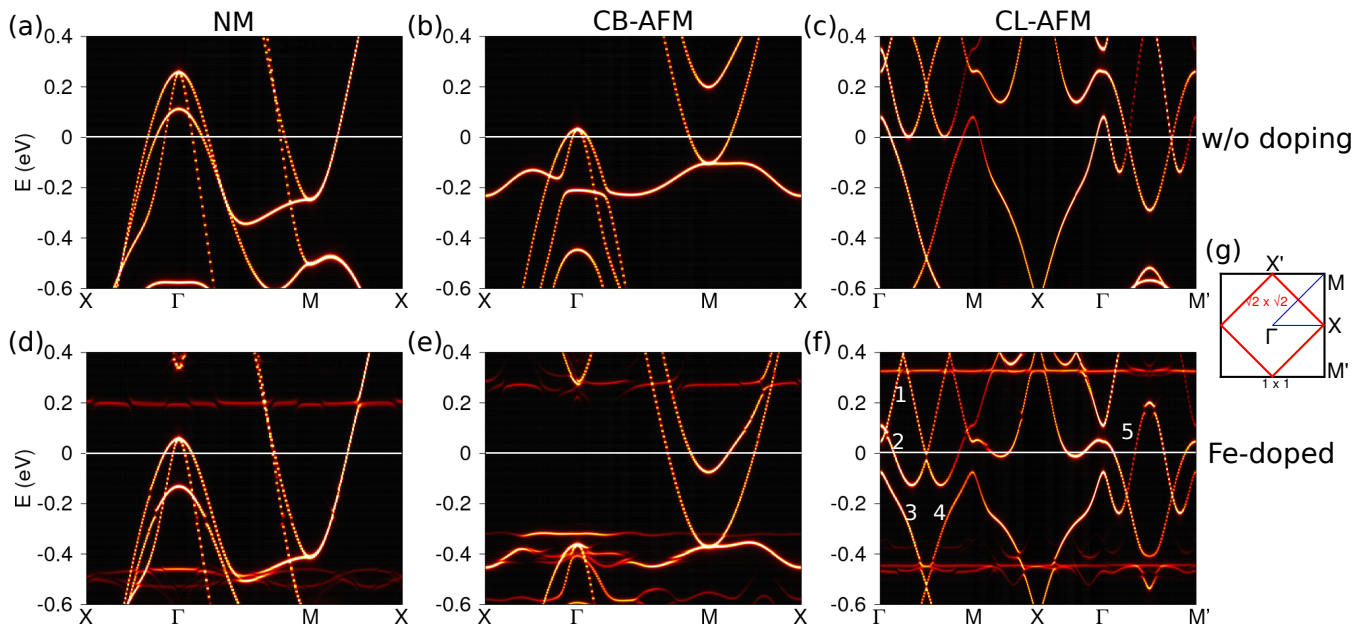
FIG. 2. k-projected bands of (a)-(c) (LiOH)FeSe and (d)-(f) (Li$_{0.8}$Fe$_{0.2}$OH)FeSe along high-symmetry lines of the BZ of the 1 × 1 unit cell shown in (g). The bands for different assumed magnetic configurations of the FeSe layer – non-magnetic (NM), checkerboard antiferromagnetic (CB-AFM), and collinear antiferromagnetic (CL-AFM) – are shown; the Fe dopants have the CL-AFM order (Fig. 1(b)). SOC was not included in these calculations and the Fermi level is set to zero. The numbers in (f) denote band indexes. (g) The BZs of the 1×1 unit cell (black) and the $\sqrt{2} \times \sqrt{2}$ supercell (red).

For the NM state the shift is about 0.2 eV. As a result, the hole pockets at Γ shrink dramatically but remain finite at E$_F$, while the electron pockets at M enlarge significantly. For the CB-AFM ordering, the doping leads to the disappearance of the hole pockets at Γ. The electron pocket at M enlarges and another electron pocket appears. A comparison of Figs. 2(b) and (e) shows that the hole-like bands at Γ are shifted down to lower energy by about 0.1 eV relative to the bottom of the electron band at M, reflecting the electronic response of the FeSe layer to the electron doping into the system. Consequently, the bandwidth is significantly reduced, from about 0.27 eV for the undoped (LiOH)FeSe to about 0.1 eV for (Li$_{0.8}$Fe$_{0.2}$OH)FeSe. This band renormalization is similar to that seen in FeSe/SrTiO$_3$(001) with interfacial oxygen vacancies.[19] (The flat bands, at around ±0.3 eV for CB-AFM, are due to the Fe dopants.)

The Fe dopants also affect the band structure for the CL-AFM state. While the chemical and magnetic unit cells for the FeSe CB-AFM ordering are the same, for the CL-AFM configuration the magnetic cell is a doubled $\sqrt{2} \times \sqrt{2}$ supercell. Because the magnetic effects on the bands are strong, the bands k-projected onto the 1×1 cell reflect the magnetic symmetry, including the repetition/folding of the bands along Γ-M (M'). (Both M and M' of the 1 × 1 BZ fold back to Γ of the $\sqrt{2} \times \sqrt{2}$ BZ; the Γ-M and Γ-M' directions differ because they correspond to k parallel or perpendicular to the ferromagnetic stripes of Fe atoms.) The intrinsic 1 × 1 chemical symmetry is reflected in the intensity differences even for the undoped

system. For example, there is an intensity difference between bands 3 and 4 along Γ-M for both (LiOH)FeSe and (Li$_{0.8}$Fe$_{0.2}$OH)FeSe, and similarly for bands 1 and 2, as well as band 5, where the band intensity changes around the mid-point of Γ-M'.

A comparison of Figs. 2(c) and (f) shows that doping 0.2 Fe to (LiOH)FeSe shifts E$_F$ by about 0.2 eV when the top of band 3 at Γ is taken as the reference. Similar to the CB-AFM case, the electron doping of the FeSe layer due to the Fe dopants induces strong band renormalization. For example, (LiOH)FeSe band 2 has a width of about 0.35 eV from its maximum at Γ to the local minimum at the k-point between Γ and M, while it is ~0.2 eV for (Li$_{0.8}$Fe$_{0.2}$OH)FeSe. Similar band renormalizations can be observed for other bands as labeled in Fig. 2(f). These results suggest that the effects of the Fe dopants in the LiOH layers are similar to those of interfacial oxygen vacancies in FeSe/SrTiO$_3$.[19]

To see how the magnetic configuration of the Fe dopants affects the electronic bands of (Li$_{0.8}$Fe$_{0.2}$OH)FeSe, calculations were also performed for CB-AFM and FM ordered dopants. The bands, with the FeSe in the CB-AFM configuration, are shown in Fig. 3. They are essentially similar to each other and to Fig. 2(e) for CL-AFM order, suggesting that the magnetic ordering of the Fe dopants has negligible effects on the band structure of the FeSe layers. (There are some noticeable differences; for example, the state nearest the Fermi level around M for the FM case is split, reflecting the fact that in the FM case there is
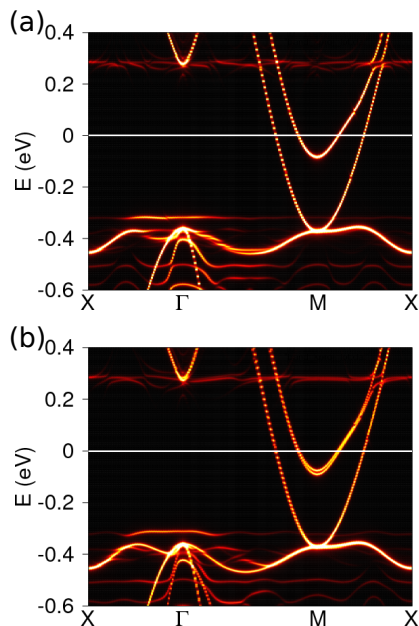
FIG. 3. k-projected bands of $(Li_{0.8}Fe_{0.2}OH)FeSe$ for different magnetic configurations of the Fe dopants: (a) CB-AFM and (b) FM. The spins in the FeSe layers have the CB-AFM ordering.
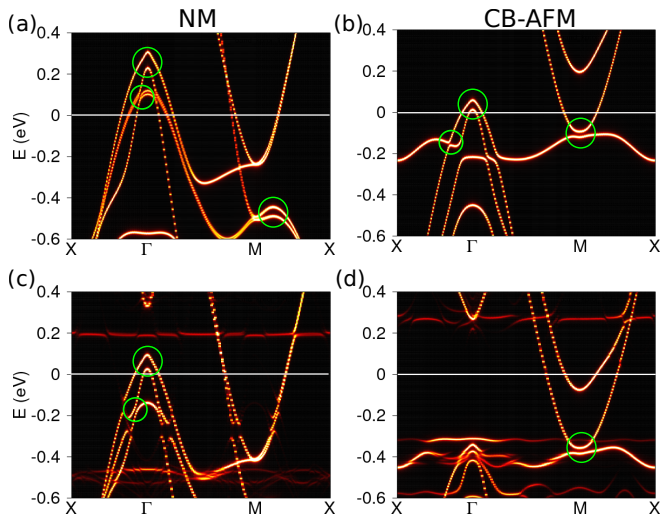
FIG. 4. Effect of spin-orbit coupling on the band structure of (a)-(b) (LiOH)FeSe and (c)-(d) $(Li_{0.8}Fe_{0.2}OH)FeSe$. Pink circles indicate the SOC splittings.

a net magnetic moment and field from the (Li,Fe)OH layer.) This insensitivity to the magnetic ordering of the dopants is not surprising since the $Li_{0.8}Fe_{0.2}OH$ and FeSe layers interact via weak vdW-like forces. Our calculations are consistent with the observation that the electronic state of $(Li_{0.84}Fe_{0.16}OH)Fe_{0.98}Se$ is highly two-dimensional.[11]

Spin-orbit coupling is of importance in Fe-based superconductors. For example, it lifts the degeneracy of the Fe d_{xz} and d_{yz} orbitals at the zone center and induces

a band splitting of over 50 meV in $Fe(Te_{0.5}Se_{0.5})$.[17] For FeSe thin films supported on $SrTiO_3(001)$, SOC induces a splitting of about 40 meV at the M point.[19] To assess the effect of SOC on $(Li_{1-x}Fe_xOH)FeSe$, calculations including SOC were performed for $(Li_{1-x}Fe_xOH)FeSe$, x = 0 and 0.2, and are shown in Fig. 4. SOC induces band splittings near Γ and M (marked by circles). For the NM state, a splitting of about 40 meV is obtained for the hole-like bands at Γ. For the CB-AFM state, a similar splitting at Γ is obtained for (LiOH)FeSe, which slightly decreases with the introduction of the Fe dopants (Fig. 4d); at the M point, the splitting is comparable to the one at Γ and is not affected by the Fe dopants. The effect of SOC on the band structure for the CL-AFM state is less prominent, due in part to the different symmetries of the wave functions, and are not shown. Although the SOC-induced splittings are dependent on the specific magnetic configurations – as are the overall band structures – they are not expected to play an important role in the superconductivity of (LiFeOH)FeSe since the relevant splitting are well away from the Fermi level.

B. Surface bands of $(Li_{0.8}Fe_{0.2}OH)FeSe(001)$

ARPES experiments observe two hole-like bands below E_F near Γ with the top of the band at about -50 meV.[12,13] Around the M point, there are parabolic electron-like bands crossing E_F with the bottom at about -60 meV, below which there are hole-like bands.[12,13] None of the above calculations produce agreement with the experiments, although the band structure for the CB-AFM state (Fig. 4(d)) is similar to the experimental observations in that there are no hole pockets around Γ and a gap appears at M. However, there are two electron pockets around M in our calculations instead of the single one observed in the ARPES experiments. Since ARPES is surface-sensitive (for photons of $\sim$20-22 eV, the expected probing depth is $\sim$5 Å[27]), the experiments of Refs. [12] and [13] will be sensitive to the surface bands of $(Li_{0.8}Fe_{0.2}OH)FeSe$, which may differ from those of the bulk.

To investigate possible changes in the band structure of $(Li_{0.8}Fe_{0.2}OH)FeSe$ at the surface, we have performed calculations for the (001) surface modeled by a FeSe-terminated slab (Fig. 5). Layer projections were performed to separate the contributions from the surface FeSe and the inner FeSe layer. Electronic bands were also unfolded using the k-projection technique. While the bands for the inner FeSe layer, Figs. 5(d-f), are essentially the same as the corresponding bulk bands in Figs. 2(d-f), the surface bands differ, especially in placement relative to the Fermi level. In all three cases, the surface bands are shifted up relative to the bulk and closer to the positioning of the bands for the undoped (LiOH)FeSe case. The simple explanation for this behavior is that the surface FeSe layer is less heavily doped since it has only one, not two, neighboring $Li_{0.8}Fe_{0.2}OH$ layers so that the
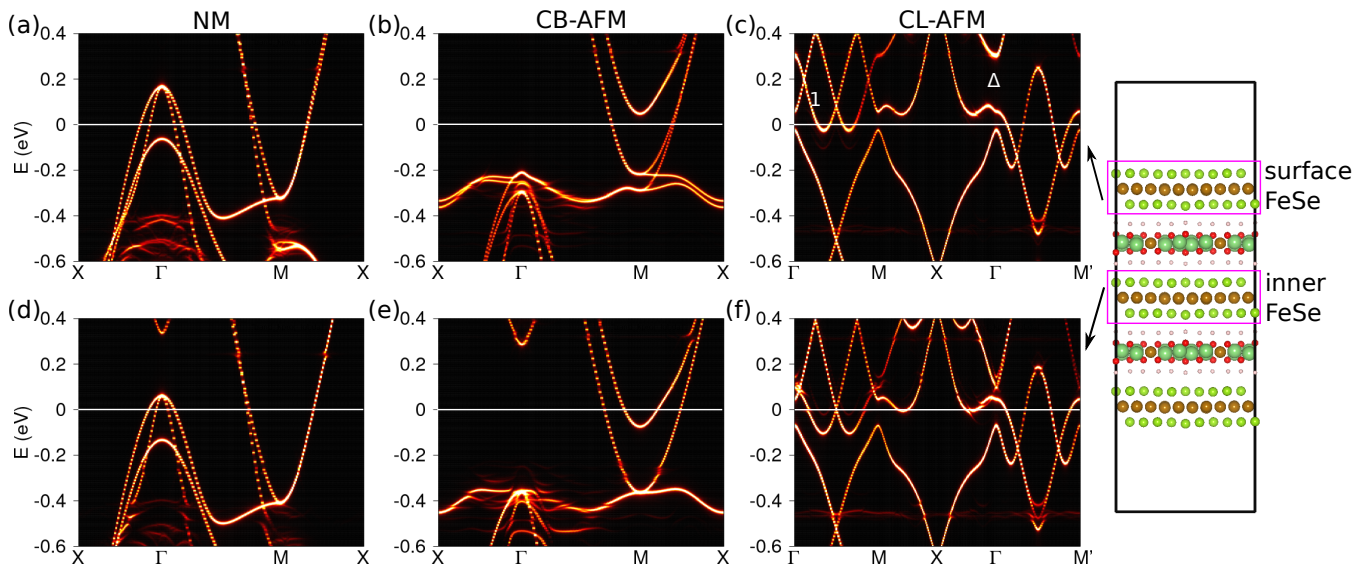
FIG. 5. k-projected bands for $(Li_{0.8}Fe_{0.2}OH)FeSe(001)$. The Fe dopants are in the CL-AFM configuration and the Fe atoms in the FeSe layers have the NM, CB-AFM and CL-AFM orderings, respectively. The Fermi level is set to zero.

surface has only approximately half the electron doping compared to the bulk. Note that the applicability of such a simple argument implicitly invokes the 2-D layered nature of both FeSe and LiOH layers, and the weak direct bonding between them. In addition to simple band filling contributions (Fermi level shifts), there are the band renormalization effects that accompany the band filling, as well as the standard surface potential shifts arising from "missing" neighbors and the modifications resulting from the lowered symmetry at the surface.

As a consequence of these effects, the hole pockets around Γ for the surface FeSe for the NM configuration are larger, whereas the electron pockets around M shrink. For the CB-AFM state around M, there is only one electron pocket, with the second one pushed up above the Fermi level. In addition, a band splitting of about 70 meV at M (located at about -0.3 eV) can be seen in the surface band structure, related to the broken inversion symmetry of the surface FeSe layer. The hole-like bands near Γ (about -0.2 eV) is closer to E_F for the surface FeSe layer than for the inner FeSe. For the CL-AFM configuration, surface effects are also noticeable, arising from similar mechanisms: Besides the shift of bands relative to E_F, the top of band 1 (Fig. 5(c)) at Γ has an upward shift, giving rise to a larger bandwidth compared to that for the inner FeSe, and the gap at Γ marked by Δ considerably increased for the surface FeSe layer.

The calculated band structure for the surface FeSe layer in the CB-AFM state (Fig. 5(b)) has similarities to the ARPES experiments, in that there is no hole pocket around Γ, only one electron pocket exists around M, and the size of the gap between the electron-like bands and the hole-like ones at the M point (along Γ-M) is comparable to the experimental value ($\sim$70 meV). However, there is a discrepancy in the Fermi level between our cal-

culations and the ARPES results: Our calculations find that E_F is about 200 meV above the top of the hole-like bands at Γ, rather than the 70 meV found in the ARPES experiments. The discrepancy could be due to defects or smaller Fe doping levels that would act to reduce the electron doping; the reported $(Li_{0.84}Fe_{0.16}OH)Fe_{0.98}Se$ in Ref. [13] would tend to go in that direction. In addition, direct comparisons of our calculations to the ARPES experiments is hindered by our neglect of final state effects and strong electron correlations that are believed might play an important role in the electronic structure of Fe-based superconductors,[28,29] particularly orbital-selective strong renormalization.[30] Moreover, SOC was not included in our calculations of the surface structure for computational reasons since the slab has a large number of atoms (240 atoms). However, as in the case of bulk $(Li_{0.8}Fe_{0.2}OH)FeSe$, the interesting SOC-induced splittings occur away from the Fermi level, and in the situations where the lower symmetry at the surface already induces a splitting, the SOC splitting is not additive,[19] and thus the calculated splittings (c.f., Fig. 5) are not expected to change dramatically.

C. Effects of Mn and Co dopings

The critical role of the Fe dopants on the high T_c superconductivity observed in $(Li_{0.8}Fe_{0.2}OH)FeSe$ and the important effects on the band structure of (LiOH)FeSe as revealed by the above calculations raise the question of how the results depend on choice of dopant, and possibly help in optimizing the superconducting T_c in $(Li_{1-x}M_xOH)FeSe$. A natural option would be the neighboring elements of Fe, i.e., Mn and Co, which by a simple electron counting are expected to give rise to differ-
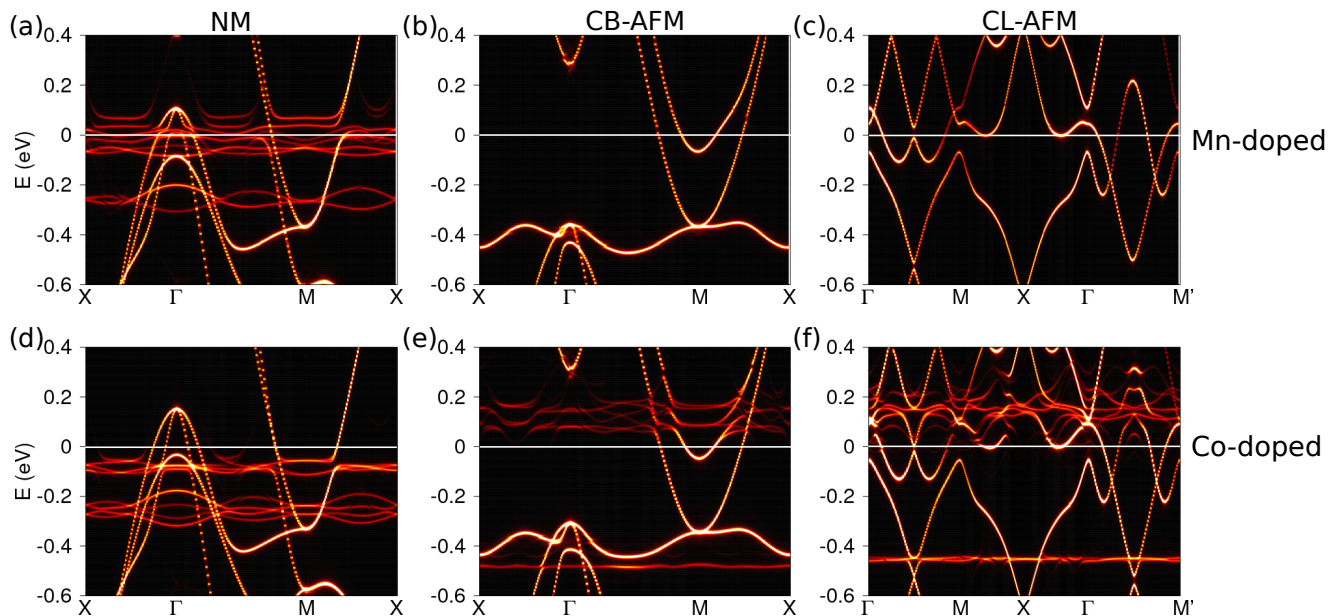
FIG. 6. k-projected bands for (a)-(c) $(Li_{0.8}Mn_{0.2}OH)FeSe$ and (d)-(f) $(Li_{0.8}Co_{0.2}OH)FeSe$. The dopants in the LiOH layer are in the CL-AFM configurations.

ent doping levels to the FeSe layer. Indeed, previous calculations show that the charge transfer between the LiOH layers and the FeSe layers is enhanced by doping Co, which may potentially increase the superconducting T_c,[15] although the increased doping is significantly

FIG. 7. Spin-resolved total density of states (solid lines) for isolated $Li_{0.8}M_{0.2}OH$, M = Li (yellow), Mn (red), Fe (green), Co (blue), calculated in the $\sqrt{5} \times \sqrt{5}$ supercell for ferromagnetic ordering of the M moments. (Antiferromagnetic coupling leads to similar *local* behavior and conclusions regarding the occupations and position of states, but the FM ordering simplifies the discussion by separating the spins.) The integrated DOS, $N(E)$, are given by the corresponding dashed lines. The different calculations were aligned using the O $2s$; the calculated Fermi level for each is denoted by the vertical dashed-dotted lines, with E_F of (Li,Fe)OH setting the overall zero.

smaller than the change in valence. To further investigate the doping effect of Mn and Co on the band structure of (LiOH)FeSe, we have also performed band unfolding calculations, Fig. 6, for both $(Li_{0.8}Mn_{0.2}OH)FeSe$ and $(Li_{0.8}Co_{0.2}OH)FeSe$, using the previously reported relaxed structures[15] and with the dopants in the LiOH layers in the CL-AFM ordering (Fig. 1(b)). Overall, the band structures for Mn- and Co-doped (LiOH)FeSe share the features of $(Li_{0.8}Fe_{0.2}OH)FeSe$. The energies of the occupied states at M for CB-AFM are unchanged for the different dopings, while at Γ there are small shifts related to the increased splitting for Co. The insensitivity of the bands to the dopant can be understood by considering the properties of the isolated LiOH spacer layer, Fig. 7, which is an insulator ($\sim$3.6 eV gap). When doped with Mn (d^5s^2), Fe (d^6s^2), or Co (d^7s^2), one of the transition-metal $4s$ electrons takes the place of the Li $2s$, albeit distorting the LiOH bands. The virtual bound states arising from the local majority d states fall in the gap region and are fully occupied. (These states are hybrids of the $3d$ orbitals and the surrounding LiOH states and have finite energy widths, but are isolated in energy. Although there are small energy differences among the different magnetic configurations, the arguments regarding the filling of minority vs. minority states still applies because the d-like states are in the gap.) For the minority d orbitals, the lowest ones filled by the remaining d electrons (0, 1, 2 for Mn, Fe, Co, respectively) are similarly in the gap. The remaining dopant electron is split between the majority LiOH conduction bands and, in the minority channel, a virtual bound d state in the LiOH conduction states; it these states that provide the doping to FeSe layer. Moreover, since the extra electrons going from Mn to Co are accommodated in (minority) gap states, the conduction

states around the Fermi level – and hence doping contributions – are similar for all three dopants. The local minority virtual bound d states are visible in Figs. 2 and 5 for Fe and Co; for Mn, the minority d states are all above the Fermi level and thus do not show up. The occupied minority "gap" state for Fe and Co doping are seen below the Fermi level. The defect level(s) above E_F corresponding to the minority d virtual bound state that is at the Fermi level for the isolated (Li,M)OH spacer layer; for Co (Fe), this state is doubly (singly) degenerate, which is reflected in these now unoccupied states. Thus, since it is the quantity rather than the type of dopant – Mn, Fe, of Co – that affects the doping level and hence electronic structure, it may be possible to tailor the dopants in order to optimize both the FeSe electronic structure and also the stability[15] of system.

IV. SUMMARY

The band structures of $(Li_{0.8}M_{0.2}OH)FeSe$ (M = Fe, Mn, Co) have been investigated via first-principles supercell calculations. The effects of doping $3d$ transition-metal elements on the band structure of FeSe layers are similar to those of interfacial oxygen vacancies in FeSe/SrTiO$_3$. The dopants provide electron doping to the FeSe layer, shifting E_F and leading to the absence of hole pockets at Γ for the checkerboard AFM state. The doping substantially modifies the profile of the Fe-$3d$ band below the Fermi level, including renormalizing band widths by a factor of about 0.3. The calculated bands for the surface layer of CB-AFM FeSe-(Li,M)OH are overall consistent with ARPES results, with the caveat that the doping levels and intrinsic defects may further modify the relative placement of the bands relative to the chemical potential. However, the band structure of the FeSe layers is insensitive to the magnetic ordering and type of dopants, suggesting the possibility of tailoring the superconducting properties by modifying the doping.

[1] Q.-Y. Wang, Z. Li, W.-H. Zhang, Z.-C. Zhang, J.-S. Zhang, W. Li, H. Ding, Y.-B. Ou, P. Deng, K. Chang, J. Wen, C.-L. Song, K. He, J.-F. Jia, S.-H. Ji, Y.-Y. Wang, L.-L. Wang, X. Chen, X.-C. Ma, and Q.-K. Xue, Chin. Phys. Lett. **29**, 037402 (2012).

[2] D. Liu, W. Zhang, D. Mou, J. He, Y.-B. Ou, Q.-Y. Wang, Z. Li, L. Wang, L. Zhao, S. He, Y. Peng, X. Liu, C. Chen, L. Yu, G. Liu, X. Dong, J. Zhang, C. Chen, Z. Xu, J. Hu, X. Chen, X. Ma, Q. Xue, and X. J. Zhou, Nat Commun **3**, 931 (2012).

[3] S. He, J. He, W. Zhang, L. Zhao, D. Liu, X. Liu, D. Mou, Y.-B. Ou, Q.-Y. Wang, Z. Li, L. Wang, Y. Peng, Y. Liu, C. Chen, L. Yu, G. Liu, X. Dong, J. Zhang, C. Chen, Z. Xu, X. Chen, X. Ma, Q. Xue, and X. J. Zhou, Nat Mater **12**, 605 (2013).

[4] S. Tan, Y. Zhang, M. Xia, Z. Ye, F. Chen, X. Xie, R. Peng, D. Xu, Q. Fan, H. Xu, J. Jiang, T. Zhang, X. Lai, T. Xiang, J. Hu, B. Xie, and D. Feng, Nat Mater **12**, 634 (2013).

[5] X. Liu, D. Liu, W. Zhang, J. He, L. Zhao, S. He, D. Mou, F. Li, C. Tang, Z. Li, L. Wang, Y. Peng, Y. Liu, C. Chen, L. Yu, G. Liu, X. Dong, J. Zhang, C. Chen, Z. Xu, X. Chen, X. Ma, Q. Xue, and X. J. Zhou, Nat Commun **5** (2014), 10.1038/ncomms6047.

[6] I. Mazin, D. J. Singh, M. D. Johannes, and M. Du, Phys. Rev. Lett. **101**, 057003 (2008).

[7] K. Kuroki, S. Onari, R. Arita, H. Usui, Y. Tanaka, H. Kontani, and H. Aoki, Phys. Rev. Lett. **101**, 087004 (2008).

[8] X. F. Lu, N. Z. Wang, H. Wu, Y. P. Wu, D. Zhao, X. Z. Zeng, X. G. Luo, T. Wu, W. Bao, G. H. Zhang, F. Q. Huang, Q. Z. Huang, and X. H. Chen, Nat. Mater. **14**, 325 (2015).

[9] U. Pachmayr, F. Nitsche, H. Luetkens, S. Kamusella, F. Brckner, R. Sarkar, H.-H. Klauss, and D. Johrendt, Angew. Chem. Int. Ed. , n/a (2014).

[10] X. Dong, H. Zhou, H. Yang, J. Yuan, K. Jin, F. Zhou, D. Yuan, L. Wei, J. Li, X. Wang, G. Zhang, and Z. Zhao, J. Am. Chem. Soc. **137**, 66 (2015).

[11] X. Dong, K. Jin, D. Yuan, H. Zhou, J. Yuan, Y. Huang, W. Hua, J. Sun, P. Zheng, W. Hu, Y. Mao, M. Ma, G. Zhang, F. Zhou, and Z. Zhao, Phys. Rev. B **92**, 064515 (2015).

[12] X. H. Niu, R. Peng, H. C. Xu, Y. J. Yan, J. Jiang, D. F. Xu, T. L. Yu, Q. Song, Z. C. Huang, Y. X. Wang, B. P. Xie, X. F. Lu, N. Z. Wang, X. H. Chen, Z. Sun, and D. L. Feng, Phys. Rev. B **92**, 060504 (2015).

[13] L. Zhao, A. Liang, D. Yuan, Y. Hu, D. Liu, J. Huang, S. He, B. Shen, Y. Xu, X. Liu, L. Yu, G. Liu, H. Zhou, Y. Huang, X. Dong, F. Zhou, K. Liu, Z. Lu, Z. Zhao, C. Chen, Z. Xu, and X. J. Zhou, Nat Commun **7**, 10608 (2016).

[14] I. A. Nekrasov and M. V. Sadovskii, JETP Lett. **101**, 47 (2015).

[15] W. Chen, C. Zeng, E. Kaxiras, and Z. Zhang, Phys. Rev. B **93**, 064517 (2016).

[16] N. Hao, Phys. Rev. X **4**, 031053 (2014).

[17] P. D. Johnson, H.-B. Yang, J. D. Rameau, G. D. Gu, Z.-H. Pan, T. Valla, M. Weinert, and A. V. Fedorov, Phys. Rev. Lett. **114**, 167001 (2015).

[18] S. V. Borisenko, D. V. Evtushinsky, Z.-H. Liu, I. Morozov, R. Kappenberger, S. Wurmehl, B. Buchner, A. N. Yaresko, T. K. Kim, M. Hoesch, T. Wolf, and N. D. Zhigadlo, Nat Phys **12**, 311 (2016).

[19] M. X. Chen, Z. Ge, Y. Y. Li, D. F. Agterberg, L. Li, and M. Weinert, Phys. Rev. B **94**, 245139 (2016).

[20] G. Kresse and J. Furthmüller, Comput. Mater. Sci. **6**, 15 (1996).

[21] G. Kresse and J. Furthmüller, Phys. Rev. B **54**, 11169 (1996).

[22] J. P. Perdew, K. Burke, and M. Ernzerhof, Phys. Rev. Lett. **77**, 3865 (1996).

[23] P. E. Blöchl, Phys. Rev. B **50**, 17953 (1994).

[24] G. Kresse and D. Joubert, Phys. Rev. B **59**, 1758 (1999).

[25] Y. Qi, S. H. Rhim, G. F. Sun, M. Weinert, and L. Li, Phys. Rev. Lett. **105**, 085502 (2010).

[26] M. X. Chen and M. Weinert, Nano. Lett. **14**, 5189 (2014).

[27] M. P. Seah and W. A. Dench, Surface and Interface Analysis **1**, 2 (1979).

[28] F. Chen, B. Zhou, Y. Zhang, J. Wei, H.-W. Ou, J.-F. Zhao, C. He, Q.-Q. Ge, M. Arita, K. Shimada, H. Namatame, M. Taniguchi, Z.-Y. Lu, J. Hu, X.-Y. Cui, and D. L. Feng, Phys. Rev. B **81**, 014526 (2010).

[29] Z. P. Yin, K. Haule, and G. Kotliar, Nat Mater **10**, 932 (2011).

[30] M. Yi, Z.-K. Liu, Y. Zhang, R. Yu, J.-X. Zhu, J. J. Lee, R. G. Moore, F. T. Schmitt, W. Li, S. C. Riggs, J.-H. Chu, B. Lv, J. Hu, M. Hashimoto, S.-K. Mo, Z. Hussain, Z. Q. Mao, C. W. Chu, I. R. Fisher, Q. Si, Z.-X. Shen, and D. H. Lu, Nat Commun **6**, 8777 (2015).